



HAL
open science

Adapted Back-EMF Sensorless Control for Permanent Magnet Synchronous Motors

Charbel Zaghrini, Gabriel Khoury, Maurice Fadel

► **To cite this version:**

Charbel Zaghrini, Gabriel Khoury, Maurice Fadel. Adapted Back-EMF Sensorless Control for Permanent Magnet Synchronous Motors. 2019 IEEE International Conference on Industrial Technology (ICIT), Feb 2019, Melbourne, Australia. pp.219-224, 10.1109/ICIT.2019.8755120 . hal-03545597

HAL Id: hal-03545597

<https://ut3-toulouseinp.hal.science/hal-03545597>

Submitted on 27 Jan 2022

HAL is a multi-disciplinary open access archive for the deposit and dissemination of scientific research documents, whether they are published or not. The documents may come from teaching and research institutions in France or abroad, or from public or private research centers.

L'archive ouverte pluridisciplinaire **HAL**, est destinée au dépôt et à la diffusion de documents scientifiques de niveau recherche, publiés ou non, émanant des établissements d'enseignement et de recherche français ou étrangers, des laboratoires publics ou privés.

Adapted Back-EMF sensorless control for Permanent Magnet Synchronous Motor

Charbel Zaghrini
ESIB, Université Saint-Joseph de
Beyrouth
Beirut, Liban
charbel.zaghrini@net.usj.edu.lb

Gabriel Khoury
CINET, ESIB, Université Saint-Joseph
de Beyrouth
Beirut, Liban
gabriel.khoury@usj.edu.lb

Maurice Fadel
LAPLACE, Université de Toulouse,
CNRS, INPT, France.
Toulouse, France
maurice.fadel@laplace.univ-tlse.fr

Abstract—This paper presents a sensorless control method for permanent magnet synchronous motors (PMSMs) based on the reconstruction of the speed and position of the rotor using the traditional method of the back-EMF with the addition of an innovative observation speed. The gains of the observer are a function of the speed and here a simple adaptation law that avoids the calculation in real time of the gains is proposed. Furthermore the speed is calculated from the back-EMF which induces a velocity oscillation due to the observation errors inherent to the sinusoidal forms. To overcome this difficulty, the direct derivation of the position is proposed taking into account the discontinuity of the position due to the modulo function. Simulation and experimental results validate the proposed method.

Keywords—PMSM, back-EMF, observers, Sensorless, Control

I. INTRODUCTION

PMSM actuators are widely used in today's industries where speed adjustment is required. In fact, the PMSMs are characterized by a possibility of adjusting the speed and the position of very high quality with an important dynamic. To achieve such a result a vector control that ensures the rigorous adjustment of the torque is developed. This vector control requires knowledge of the position of the rotor and thus the machines are equipped with a resolver type position or absolute optical encoder. This sensor is usually expensive and results in an increased probability of failure. Moreover, its presence is not desirable in several types of application because of the constraints it imposes on the mechanical or electrical. From there, a number of manufacturers have been interested in removing this sensor and trying to achieve sensorless control.

The sensorless control of synchronous machines is therefore an old theme that has given rise to numerous publications [1], [2], [3], [4]. There are several principles depending on the required performance, the type of application.

In this paper, an observer based on the reconstruction of electromotive forces is developed and a simple solution improving the estimated velocity is developed.

The usual methods consist in reconstructing the back-emf with the aid of a Luenberger observer, then in determining the operating speed by combination of the two back-emf. This solution is characterized by speed ripple inherent to the EMF reconstruction and affects the amplitude. In this paper a procedure of direct derivation of the position taking into account the discontinuity is developed in order to keep the response as smooth as possible. The proposed solution provides a results closer to the actual speed which improves

the overall control. Simulation and experimental results are presented, and validate the proposed method.

II. FIELD ORIENTED CONTROL

A. Field oriented control concept

The basic idea of the vector control algorithm is to decompose a stator current into two components: A magnetic field generating-part and a torque-generating part [5], [6]. Both components can be controlled separately once decoupled. In this paper, effort is carried on the torque generation to reach the required objective. The machine being smooth pole, the maximum torque is obtained for a given current by imposing a zero current on the axis d.

B. Control system

Park transformation is used to transform the 3-phase time-domain stator currents from a stationary phase coordinate (abc) to a rotating coordinate system (dq). The d-axis current (image of the magnetic flux) and the q-axis current (image of the torque) are controlled by PI regulators. The reference for the d-axis current is set to 0 and the q-axis reference is generated by a speed PI regulator. A voltage inverter with three legs connected to the three phases of the PMSM is used. Each leg has two switches each consisting of an IGBT and an antiparallel diode controlled by the space vector modulation (SVM).

C. Position and speed sensing

The control system needs the rotor's position and speed feedback which are usually provided by a mechanical sensor. The paper objective is to replace this sensor by a system that estimates the position and the speed of the motor and then feeding the control with the estimated data. The system that will be presented uses the equations of the PMSM and the electromotive forces induced in the stator windings and is known by "Back-EMF based observer" [7], [8], [9].

III. BACK-EMF BASED OBSERVER

Different types of observers can be found in the literature [3], [9], [10]. There is the Phased Locked Loop (PLL) type and the state-space observers. Among these observers, there is two families, the Kalman filter and the Luenberger observer. The latter observer (Back-EMF) will be developed for it is less expensive in term of calculations compared to the Kalman filter. The dynamics of the machine being a function of the speed, the gains of the observer also depend on the speed. To avoid the real-time calculation it is possible to adapt the gains directly after an offline study.

A. Mathematical model of a PMSM for Back-EMF estimation

To set up a state-space observer, the state-space equations associated to the state-space variables are written. For the PMSM, the currents in the stator windings are found as state-space variables and the electromotive forces are included since these are the variables that need to be observed. The state-space equations will be written down in the $\alpha\beta$ domain to get a useful estimation of the electromotive forces. In order to build the model, a sinusoidal distribution for the magnetomotive force is taken into consideration and the saturation phenomena in the iron is neglected. Thus, the electrical behavior of the motor is defined by:

$$V_{abc} = \frac{d\varphi_{abc}}{dt} + R_s \cdot I_{abc} \quad (1)$$

The flux of the motor φ_{abc} is composed of the flux of the permanent magnet adding to it the flux created by the currents in the stator windings. φ_{abc} is given by:

$$\varphi_{abc} = \begin{bmatrix} \cos(\theta_e) \\ \cos\left(\theta_e - \frac{2\pi}{3}\right) \\ \cos\left(\theta_e + \frac{2\pi}{3}\right) \end{bmatrix} \cdot \varphi_f + L_s \cdot I_{abc} \quad (2)$$

The motor's equations are now written in the $\alpha\beta$ frame. After applying the Clarke transform on the equations (1) and (2), the following relationships appear:

$$V_\alpha = \frac{d\varphi_\alpha}{dt} + R_s \cdot I_\alpha \quad (3)$$

$$V_\beta = \frac{d\varphi_\beta}{dt} + R_s \cdot I_\beta \quad (4)$$

$$\begin{cases} \varphi_\alpha = \cos(\theta_e) \cdot \varphi_f + L_s \cdot I_\alpha \\ \varphi_\beta = \sin(\theta_e) \cdot \varphi_f + L_s \cdot I_\beta \end{cases} \quad (5)$$

Where:

V_{abc} stator voltages in the stationary abc frame

φ_{abc} stator flux in the stationary abc frame

R_s stator resistance

I_{abc} stator currents in the stationary abc frame

V_α, V_β stator voltages in the stationary $\alpha\beta$ frame

$\varphi_\alpha, \varphi_\beta$ stator flux in the stationary $\alpha\beta$ frame

I_α, I_β stator currents in the stationary $\alpha\beta$ frame

φ_f permanent magnet flux linkage

L_s stator inductance

θ_e rotor's electrical position

B. Mathematical model of the state-space observer

In order to write the state-space equations, in (3) and (4). This will lead to

$$\begin{cases} \dot{I}_\alpha = -\frac{R_s}{L_s} \cdot I_\alpha + \frac{1}{L_s} \cdot \varphi_f \cdot \omega_e \cdot \sin(\theta_e) + \frac{V_\alpha}{L_s} \\ \dot{I}_\beta = -\frac{R_s}{L_s} \cdot I_\beta - \frac{1}{L_s} \cdot \varphi_f \cdot \omega_e \cdot \cos(\theta_e) + \frac{V_\beta}{L_s} \end{cases} \quad (6)$$

Where:

ω_e rotor's electrical velocity

The equations of the electromotive forces in the $\alpha\beta$ domain are identified in (6) and can be written in the following form:

$$\begin{cases} E_\alpha = -\omega_e \cdot \varphi_f \cdot \sin(\theta_e) \\ E_\beta = \omega_e \cdot \varphi_f \cdot \cos(\theta_e) \end{cases} \quad (7)$$

Where:

E_α, E_β electromotive forces in the stationary $\alpha\beta$ domain

Equation (6) can now be written in this form:

$$\begin{cases} \dot{I}_\alpha = -\frac{R_s}{L_s} \cdot I_\alpha - \frac{1}{L_s} \cdot E_\alpha + \frac{V_\alpha}{L_s} \\ \dot{I}_\beta = -\frac{R_s}{L_s} \cdot I_\beta - \frac{1}{L_s} \cdot E_\beta + \frac{V_\beta}{L_s} \end{cases} \quad (8)$$

The objective is to observe the electromotive forces. The state-space vector will be $[I_\alpha \ I_\beta \ E_\alpha \ E_\beta]^T$. Therefore, the derivatives of the EMFs need to be calculated in order to write the system in a matrix form. Deriving (7) leads to:

$$\begin{cases} \dot{E}_\alpha = -\omega_e^2 \cdot \varphi_f \cdot \cos(\theta_e) = -\omega_e \cdot E_\beta \\ \dot{E}_\beta = \omega_e^2 \cdot \varphi_f \cdot \sin(\theta_e) = \omega_e \cdot E_\alpha \end{cases} \quad (9)$$

The system can now be written in this form:

$$\begin{cases} \dot{X} = A \cdot X + B \cdot U \\ Y = C \cdot X \end{cases} \quad (10)$$

Where U is the input vector (V_α and V_β) and Y is the output vector (I_α and I_β). By considering X the state-space vector mentioned above, (10) can be developed in order to have:

$$\begin{bmatrix} \dot{I}_\alpha \\ \dot{I}_\beta \\ \dot{E}_\alpha \\ \dot{E}_\beta \end{bmatrix} = \begin{bmatrix} -\frac{R_s}{L_s} & 0 & -\frac{1}{L_s} & 0 \\ 0 & -\frac{R_s}{L_s} & 0 & -\frac{1}{L_s} \\ 0 & 0 & 0 & -\omega_e \\ 0 & 0 & \omega_e & 0 \end{bmatrix} \cdot \begin{bmatrix} I_\alpha \\ I_\beta \\ E_\alpha \\ E_\beta \end{bmatrix} \quad (11)$$

$$Y = \begin{bmatrix} 1 & 0 & 0 & 0 \\ 0 & 1 & 0 & 0 \end{bmatrix} \cdot X + \begin{bmatrix} \frac{1}{L_s} & 0 \\ 0 & \frac{1}{L_s} \\ 0 & 0 \\ 0 & 0 \end{bmatrix} \cdot \begin{bmatrix} V_\alpha \\ V_\beta \end{bmatrix} \quad (12)$$

Using (11) and (12) the matrixes A, B and C can be easily identified and will be useful later on. Manipulating the equations in (7) leads to:

$$\hat{\theta}_e = \tan^{-1}\left(-\frac{E_\alpha}{E_\beta}\right) \quad (13)$$

$$\hat{\omega}_e = \frac{1}{\varphi_f} \cdot \sqrt{E_\alpha^2 + E_\beta^2} \quad (14)$$

Where:

$\hat{\theta}_e$ estimated position given by the observer
 $\hat{\omega}_e$ estimated speed given by the observer

Thus, by observing the EMFs along the α and β axis, it is possible to determine the position and the speed via (13) and (14) respectively.

In order to have a good estimation, the currents I_α and I_β calculated by the observer need to be regulated so that they converge towards the real currents of the motor.

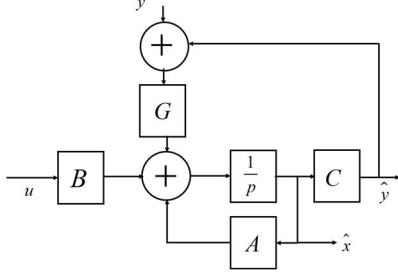


Fig. 1. Principle of the state-space observer

The observer relies on the comparison between the real measurements of the matrix Y (which are the currents I_α and I_β obtained from the phase currents I_a , I_b and I_c measured) and the estimated measurements of the matrix \hat{Y} (the currents estimated by the observer in the $\alpha\beta$ frame). The error obtained is sent in a matrix called G in Fig. 1. This matrix has for role to converge the error towards 0 (like a normal regulator). Using Fig.2 the system's state-space equation in closed loop can be written down:

$$\frac{d\hat{X}}{dt} = (A - G.C). \hat{X} + B.U + G.Y \quad (15)$$

As for a normal regulator, the dynamics of the system in closed loop should be placed. Therefore, G needs to be computed in order to place the eigenvalues of the matrix $(A - G.C)$. 4 poles need to be calculated for a 4th order system. This can be done by solving this equation:

$$\det(\lambda.I - (A - G.C)) = (\lambda - \lambda_1) \cdot (\lambda - \lambda_2) \cdot (\lambda - \lambda_3) \cdot (\lambda - \lambda_4) \quad (16)$$

Here: $\lambda_1, \lambda_2, \lambda_3, \lambda_4$ are the desired poles

To simplify the problem, assumptions were taken into consideration: $\lambda_2 = \bar{\lambda}_1$ (conjugate) and the poles were chosen to be double and purely reals. That leads to $\lambda_1 = \lambda_3$ and $\lambda_2 = \lambda_4$. Combining $\lambda_1 = a_1 + j.b_1$ with the assumptions made leads to having $\lambda_1 = \lambda_2 = \lambda_3 = \lambda_4 = a_1$ (4 identical real poles). The constant a_1 must be chosen carefully for this is the parameter that will control the dynamics of the observer. a_1 must have a negative value to ensure the stability of the closed-loop system, plus taking into consideration that the observer must calculate the estimated speed faster than the calculations made by the regulator of the speed loop in order to have a good and reliable estimation. To satisfy these requirements, the biggest pole of the speed loop transfer function is multiplied by a number (based on the speed needed for the observer in term of calculations). If the pole is complex real part of it is taken. This number have a limit based on the speed of the IGBTs in the inverter.

Now that the poles have been set, the matrix's G elements can be calculated. G has the following form:

$$\begin{pmatrix} g_{11} & g_{12} \\ g_{21} & g_{22} \\ g_{31} & g_{32} \\ g_{41} & g_{42} \end{pmatrix} \quad (17)$$

Since only 4 poles have to be calculated, symmetries can be used to simplify the element's calculations. The two matrixes I and J are introduced:

$$I = \begin{bmatrix} 1 & 0 \\ 0 & 1 \end{bmatrix} \text{ and } J = \begin{bmatrix} 0 & -1 \\ -1 & 0 \end{bmatrix} \quad (18)$$

After using (18), the matrix G will have the following form:

$$G = \begin{bmatrix} g_{11}.I + g_{12}.J \\ g_{31}.I + g_{32}.J \end{bmatrix} \quad (19)$$

That leads to having: $g_{11} = g_{22} = g_1$, $g_{21} = -g_{12} = g_3$, $g_{31} = g_{42} = g_2$ and $g_{41} = -g_{32} = g_4$

Using the assumptions made earlier on the poles, (16) can be written in this form:

$$\det(\lambda.I - (A - G.C)) = (\lambda - \lambda_1)^4 \quad (20)$$

Developing (20) will lead to:

$$\det(\lambda.I - (A - G.C)) = \lambda^4 - \lambda^3 \cdot 4a_1 + \lambda^2 \cdot 6a_1^2 - \lambda \cdot 4a_1^3 + a_1^4 \quad (21)$$

Equation (21) can be coded and solved using Matlab. Solving this equation gets the matrix's elements shown in the following relations:

This formulation makes it possible to adapt in real time the gains of the observer as a function of speed.

$$g_1 = -\frac{R_s}{L_s} - 2a_1 \quad (22)$$

$$g_2 = \omega_e \quad (23)$$

$$g_3 = L_s \cdot (\omega_e^2 - a_1^2) \quad (24)$$

$$g_4 = 2L_s \omega_e a_1 \quad (25)$$

C. Simulation results

After implementing the observer's model on Simulink, tests were carried. An initial angle was given to the motor to see if the observer can catch up with the rotor's actual position.

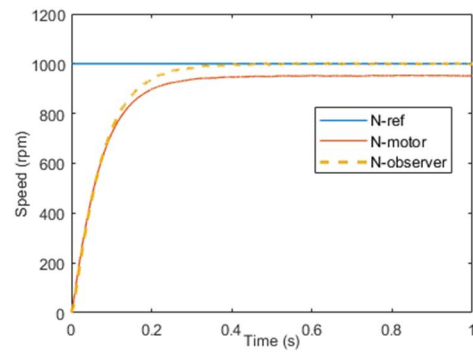


Fig. 2. Real speed of the machine (red graph) versus the estimated speed (yellow graph) without load for an initial position of 50 degrees.

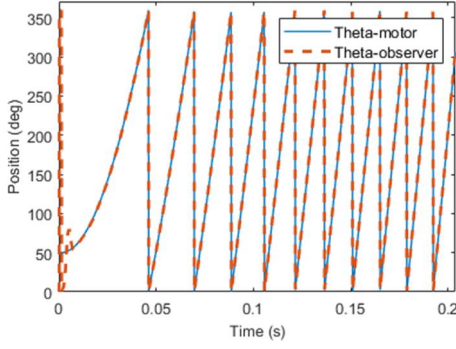


Fig. 3. Real speed of the machine (red graph) versus the estimated speed (yellow graph) without load for an initial position of 50 degrees.

Fig. 3 shows that the observer's estimated position starts at 0 and catch up with the actual motor's position within 0.008s which is compliant to the dynamics imposed ($7.75/a1$). Fig. 2 shows a steady-state error of 5% between the real and the estimated speed curves. To investigate this error, tests were done with a load of 0.2 Nm and for a speed reference of 500 rpm (from 0 to 1s) and 1000 rpm (form 1 to 2s).

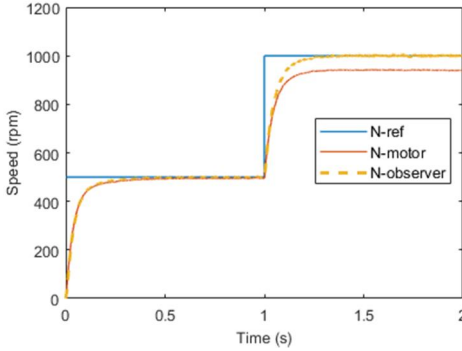


Fig. 4. Real speed of the machine (red graph) versus the estimated speed (yellow graph) with a load of 0.2 Nm

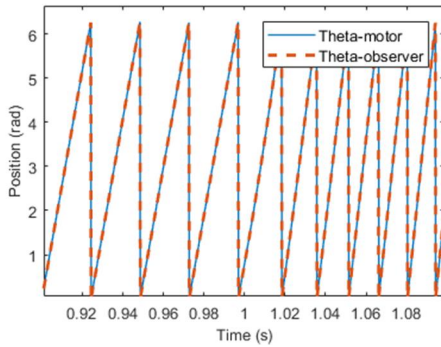


Fig. 5. Real position of the machine (blue graph) versus the estimated position (red graph) with a load of 0.2 Nm

Fig. 4 shows that the error on the speed curves increases with the speed imposed. For a 500 rpm speed reference the error is 1% while the error for the 1000 rpm speed reference is 6%. It is also noticeable that the error increases with the load. Fig. 2 shows an error of 5% without load while it increased to 6% after applying a resistive torque in Fig. 4. The position curves on the other hand are perfectly superposed for the two speed references as shown in Fig. 5.

D. Experimental results

To verify the effectiveness of the analyses made on the Back-EMF observer, experiments were performed on a 1.4

kW PMSM powered by a DC voltage source via a two-stage three-phase inverter (switching frequency of 7Khz) and coupled to an identical machine that will play the role of the load. This machine will run as a generator and will dissipate the energy produced in a resistor. It is driven by its own inverter to control the speed of the load and create an opposing torque on the motor. Fig. 5 is a photo showing the two coupled PMSMs. The real position of the motor (that will be compared to the estimated position of the observer) is measured using a synchro-resolver. The parameters of the PMSM are listed in Table I.



Fig. 4. The tested PMSM (left) coupled to the load motor (right)

TABLE I. 1.4-kW PMSM PARAMETERS

φ_f	$3.45 \cdot 10^{-2}$ Wb
L_s	5.65 mH
R_s	1.35 Ω
Pair of poles	5
DC source voltage	50 V
Maximum speed	1600 rpm

The results were taken using the highest dynamics reached on the test bench ($a1=50$ pole).

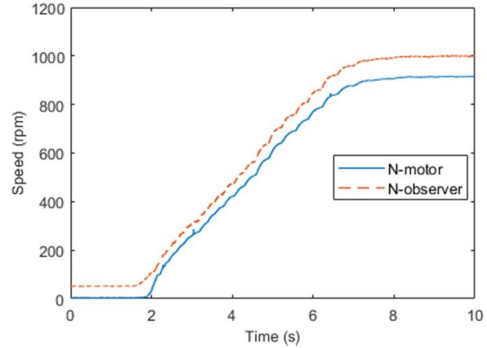


Fig. 6. Real speed of the machine (red graph) versus the estimated speed (yellow graph) for a speed reference of 1000 rpm (blue graph) without load

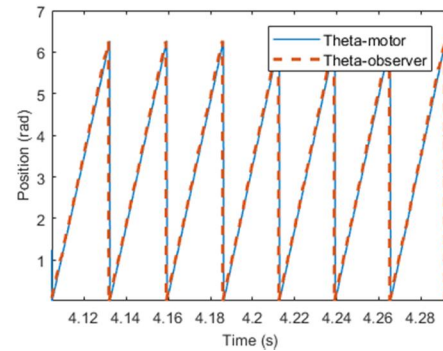


Fig. 7. Real position of the machine (blue graph) versus the estimated position (red graph) for a speed reference of 1000 rpm without load

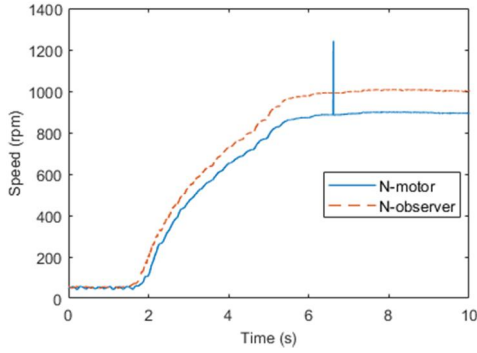


Fig. 8. Real speed of the machine (red graph) versus the estimated speed (yellow graph) for a speed reference of 1000 rpm (blue graph) with a load of 0.2 Nm

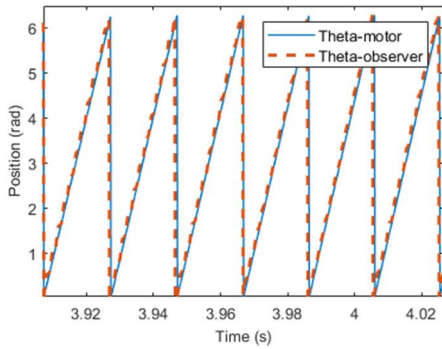


Fig. 9. Real position of the machine (blue graph) versus the estimated position (red graph) for a speed reference of 1000 rpm with a load of 0.2 Nm

It is possible to see that the experimental results are in agreement with the simulation ones. The steady-state error is clearly noticeable in Fig. 6 and Fig. 8. The positions in Fig. 7 and Fig. 9 are not affected by the error and the graphs are well superposed. Furthermore, the amplitude of the error increased compared to the simulation values. Without applying a resistive torque, Fig. 6 shows an error of 8.5% and for a resistive torque of 0.2 Nm Fig. 8 shows an error of 10%.

One way to find the origin of this steady-state error is to return to the estimated speed relation in (14). The speed depends on the square of the electromotive forces along the $\alpha\beta$ axis. A slight error on these variables can cause a large one on the estimated speed. E_α can be compared to its theoretical value in (7) for a 1000 rpm speed reference using different dynamics (the results seen on E_α are images of those on E_β since the latter is a cosinusoidal image of E_α).

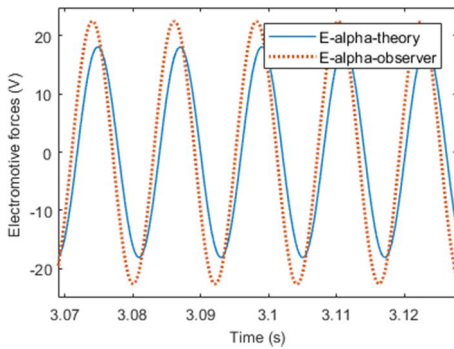


Fig. 10. Electromotive forces along α -axis calculated by the observer (blue graph) versus their theoretical value (red graph) for $l=50$

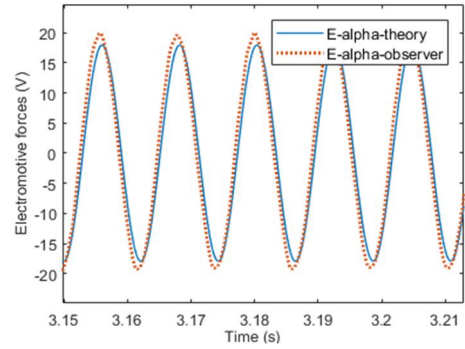


Fig. 11. Electromotive force along α -axis calculated by the observer (blue graph) versus its theoretical value (red graph) for $l=150$

Fig. 10 shows that for slow dynamics a considerable phase shift and an amplitude offset appear between the curves. The difference between the electromotive forces obtained and their theoretical values will induce an offset between the estimated speed given by the observer and the real speed due to (14). Fig. 11 shows that increasing the dynamics of the observer tend to decrease the phase shift and the magnitude offset between the calculated EMFs and their theoretical values which will lead to a better precision.

IV. BACK-EMF MODIFIED FOR BETTER PRECISION

In order to eliminate the steady-state error on the speed without having to increase the dynamics of the observer, a simple modification is introduced on the system and tested in simulations. Experimental results will be available in the next paper when works on the test bench are done.

A. Deriving the position

According to the simulation and experimental results shown above, the estimated position is not affected by the errors on the electromotive forces and follows the real position of the machine for all the speed reference cases. The modification made consists in the reconstruction of the position only and then deduce the speed by deriving the position.

As the position is calculated in “modulo 2π ”, the velocity is obtained by derivation of the position (using Euler’s method) ignoring the discontinuities (from 2π to 0). The code used for the implementation of the derivative function is shown in Fig.12. The speed is then filtered by a first-order filter in order to remove the unwanted frequency components coming from the infinite values calculated by the derivative function. Using a low frequency pass filter would introduce an undesirable phase shift into the control if its bandwidth is low, and would be useless if its bandwidth is high. A Kalman filter that estimates the time variables taking into account the measurement noise can also be used. The bandwidth of the first-order filter is set to 35 Hz. The schematic diagram of the modified system and the code used to create the derivative function is shown in Fig. 12.

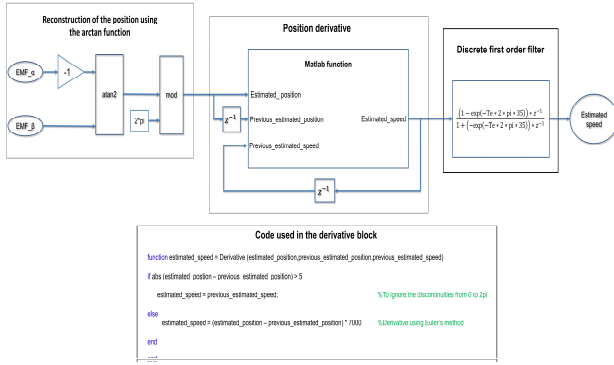


Fig. 12. Schematic diagram of the modified system with the code used to create the derivative function

In the first two lines of the code a simple test is used to eliminate the discontinuity from 0 to 2π . For the derivative part the Euler's derivative method shown in the relation below is used:

$$\begin{aligned} \frac{dx}{dt} &= \frac{x(k) - x(k-1)}{T_e} \\ &= (x(k) - x(k-1)) * F_e \end{aligned} \quad (26)$$

Where T_e is the sampling time and F_e the corresponding sampling frequency ($F_e = \frac{1}{T_e}$) which is equal to the cutting frequency of the inverter (7KHz).

B. Simulation results after deriving the position

To see the effectiveness of the modification made, the estimated and real velocity are plotted for the same speed references used in simulations with a resistive torque of 0.2 Nm (which was the worst case in the simulation results).

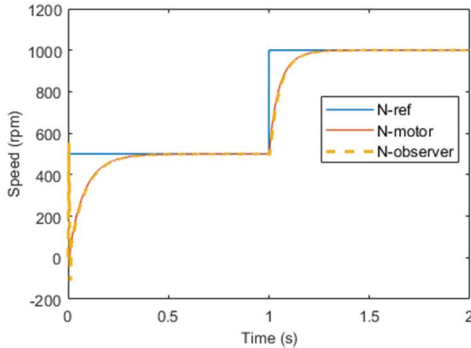


Fig. 13. Real speed of the machine (red graph) versus the estimated speed (yellow graph) with a load of 0.2 Nm

Fig. 13 shows that the steady-state error between the estimated speed graph and the real speed graph is entirely gone for the two speed references. The graphs now perfectly coincide at steady-state with an inconsiderable phase shift between them in the transient phase caused by the low-pass filter. Thus, deriving the position appears to be good method to improve the precision of the observer without having to go fast in the dynamics.

This article is dedicated to the mechanical sensorless control of a PMSM. More precisely, he wants to recreate the position and speed of rotation in a simple and efficient way. The solution is based on the electromotive forces and on the use of an arctangent function. The peculiarity lies in 2 contributions. The first is related to an offline study which allowed to give a law of simple evolution of the parameters of the observer according to the speed. This avoids real-time quantization of the eigenvalues of a 4-dimensional matrix. The second is to determine the filtered bypass velocity of the position which makes it possible to eliminate the influence of the observation errors of the emfs in amplitude and in phase on the value of the speed. This solution has been validated by simulation and is currently undergoing an experimental verification that will be presented in the final version.

This simple method is applicable to any type of synchronous machine.

VI. REFERENCES

- [1] Zhiqian Chen, M. Tomita, S. Doki and S. Okuma. An extended electromotive force model for sensorless control of interior permanent-magnet synchronous motors. *IEEE Transactions on*, vol. 50, no. 2, pages 288–295, Apr 2003.
- [2] Shigeo Morimoto, Keisuke Kawamoto, Masayuki Sanada and Yoji Takeda. Sensorless control strategy for salient-pole PMSM based on extended EMF in rotating reference frame. In *Industry Applications Conference, 2001. Thirty-Sixth IAS Annual Meeting. Conference Record of the 2001 IEEE*, volume 4, pages 2637–2644. IEEE, 2001.
- [3] Silverio Bolognani, Sandro Calligaro and Roberto Petrella. Design issues and estimation errors analysis of back-EMF-based position and speed observer for SPM synchronous motors. *IEEE Journal of Emerging and Selected Topics in Power Electronics*, vol. 2, no. 2, pages 159–170, 2014.
- [4] Sidath Diao, Demba Diallo, Zatar Makni, Claude Marchand and Jean-Francois Bisson. A differential algebraic estimator for sensorless permanent-magnet synchronous machine drive. *IEEE Transactions on Energy Conversion*, vol. 30, no. 1, pages 82–89, 2015.
- [5] A. Zgorski, B. Bayon, G. Scorletti and Xuefang Lin-Shi. LPV observer for PMSM with systematic gain design via convex optimization, and its extension for standstill estimation of the position without saliency. In *Sensorless Control for Electrical Drives (SLED), 2012 IEEE Symposium on*, pages 1–6, Sept 2012.
- [6] Corley, M. J. and Lorenz, R.D. Rotor position and velocity estimation for a salient-pole permanent magnet synchronous machine at standstill and high speeds. In: *IEEE Transactions on Industry Applications* vol. 34 (1998), Nr. 4, 784–789
- [7] Youness Aite driss, Driss Yousfi. PMSM Sensorless Control using Back-EMF Based Position and Speed Estimation Method, 2013 *International Renewable and Sustainable Energy Conference (IRSEC)*, 7-9 March 2013.
- [8] Xinlong Zhang, Guangyu Tian, Yong Huang and Ziwang Lu. A Comparative Study of PMSM Sensorless Control Algorithms: Model Based vs Luenberger Observer, 17-20 Oct. 2016, 2016 *IEEE Vehicle Power and Propulsion Conference (VPPC)*.
- [9] Zheng Zedong, Maurice Fadel, Li Yongdong, "Sensorless Control of PMSM Based on Extended Kalman Filter" 2007 *EPE 2007 AALBORG (Danemark) 02/09/2007 au //05/09/2007*
- [10] Kwang-Woon Lee, Jung-Ik Ha. Evaluation of Back-EMF Estimators for Sensorless Control of Permanent Magnet Synchronous Motors. *Journal of Power Electronics*, Vol. 12, No. 4, July 2012